U. S. Naval Research Laboratory
Washington, DC 20375-5320

NRL/5340/MR--2021/10

An Explicit Bistatic Glint Solution for an Arbitrary Number of Scatterers Using the Phase Gradient Method

David Frederic Crouse

Surveillance Technology Branch
Radar Division

December 29, 2021

REPORT DOCUMENTATION PAGE

Form Approved
OMB No. 0704-0188

1. REPORT DATE (DD-MM-YYYY)	2. REPORT TYPE	3. DATES COVERED (From – To)
29-12-2021	NRL Memorandum Report	

4. TITLE AND SUBTITLE

An Explicit Bistatic Glint Solution for an Arbitrary Number of Scatterers Using the Phase Gradient Method

5a. CONTRACT NUMBER

5b. GRANT NUMBER

5c. PROGRAM ELEMENT NUMBER
63801N

6. AUTHOR(S)

David Frederic Crouse

5d. PROJECT NUMBER

5e. TASK NUMBER

5f. WORK UNIT NUMBER
1R68

7. PERFORMING ORGANIZATION NAME(S) AND ADDRESS(ES)

U. S. Naval Research Laboratory
4555 Overlook Avenue, SW
Washington, DC 20375-5320

8. PERFORMING ORGANIZATION REPORT NUMBER

NRL/5340/MR - - 2021/10

9. SPONSORING / MONITORING AGENCY NAME(S) AND ADDRESS(ES)

Office of Naval Research
One Liberty Center
875 N. Randolph Street, Suite 1425
Arlington, VA 22203-1995

10. SPONSOR / MONITOR'S ACRONYM(S)
ONR

11. SPONSOR / MONITOR'S REPORT NUMBER(S)

12. DISTRIBUTION / AVAILABILITY STATEMENT
Distribution Statement A: Approved for public release. Distribution is unlimited.

13. SUPPLEMENTARY NOTES

14. ABSTRACT
Given multiple unresolved scatterers in range, Doppler, and angle, estimation techniques that assume that only a single target is present, such as traditional monopulse estimation, are well known to produce biased estimates, particularly in angle. This paper derives the apparent target location and range rate in the presence of multiple scatterers utilizing the phase gradient method. The solution is given in 2D/3D Cartesian coordinates. Additionally, bounds on the maximum and minimum errors are given in 2D for the two-scatterer problem.

15. SUBJECT TERMS
Glint, scintillation, unresolved targets, radar

16. SECURITY CLASSIFICATION OF:			17. LIMITATION OF ABSTRACT	18. NUMBER OF PAGES	19a. NAME OF RESPONSIBLE PERSON
a. REPORT	b. ABSTRACT	c. THIS PAGE			David F. Crouse
U	U	U	U	19	19b. TELEPHONE NUMBER *(Include area code)* 202-404-1859

Standard Form 298 (Rev. 8-98)
Prescribed by ANSI Std. Z39.18

This page intentionally left blank

CONTENTS

AN EXPLICIT BISTATIC GLINT SOLUTION FOR AN ARBITRARY NUMBER OF SCATTERERS USING THE PHASE GRADIENT METHOD

1. INTRODUCTION

When considering the tracking of targets, by radar, it is often convenient to model individual targets as single points and that separate targets will always produce separate (resolved) detections. However, in many instances, such a single-point approximation is insufficient. When multiple closely-spaced targets, or multiple scatterers on a single target, are unresolved in angle, range, and range-rate, and superresolution algorithms are not used, measurements can be biased, with biases and measurement amplitudes varying notably over time. The biases are known as "glint" and the amplitude variations are deemed "scintillation." This report provides explicit formulae for the apparent location and range rate of a group of unresolved moving scatterers in a bistatic measurement system under a narrowband model and a single polarization.

Though true targets are complex, extended structures that produce complicated resonant returns [1], it can be mathematically convenient to represent a single target (or a collection of unresolved targets) as a collection of non-interacting discrete scatterers (points) in space whose returns can be described as the superposition of the returns of each individual scatterer. Such discrete scatterer models have been used to describe glint errors going into target tracking algorithms [2].

Some of the oldest models describing radar returns that have been corrupted with glint (when expecting only a single resolved target) are stochastic in nature [3], [4]. Real data has shown that noisy glint-corrupted measurements are not well modeled using Gaussian probability distributions, but rather require distribution with long tails [5]. Stochastic modeling has continued to the present day leading to the development of target tracking algorithmic components in the presence of glint such as in [5–10]. Interestingly, the target tracking literature has treated the problem of tracking in the presence of glint independently of that of tracking unresolved targets. The tracking of unresolved targets typically focusses on the problem of assigning a single measurement to multiple targets. However, in numerous publications on unresolved target tracking [11–15], [16, Ch. 7.1], it is simply assumed that the mean apparent measurement of the two unresolved targets is the weighted average of their individual noise free measurement components. However, that is not how glint behaves and the unresolved tracking literature might be able to benefit from the inclusion of glint models.

For modeling the effects of glint for the purpose of target tracking simulations, the use of a deterministic model based on individual point scatterers can be useful: scatterers can be positioned representing real target geometries and the geometries of scatterers on real targets. Additionally, the computation of glint-biased measurements under such models is fast and simple and can be used as a minimal basis of validating the choice of stochastic parameters in glint-aware tracking filters in the absense of real data. Though higher-fidelity glint models, such as [17], utilizing more advanced target models exist, we choose the scattering point model here, since it can be used without recourse to detailed models of the shape of targets.

The modeling of glint implicitly assumes that superresolution algorithms that detect and estimate the presence of more than one target, such as [18–21] are not used. At the same time, it is assumed that some

Manuscript approved December 23, 2021.

type of refined estimation besides performing detections over range-range-Doppler beams is done. While this might be a form of generalized monopulse estimation in angle [22], such refine is also possible in range and Doppler, as in [23] and as one can infer from the Barankin bounds of range estimates, which can be far lower than the accuracy implied by the range resolution of a radar [24]. If no such refinement is performed in range and Doppler, then one would not expect the analysis of this paper to necessarily be valid for the errors produced there.

Given a set of non-interacting scatterers that cannot be resolved in range, range-rate, and angle by a radar, and assuming that no algorithms for detecting the presence of unresolved targets is used and that only a single polarization is used in detection, the two most prevant techniques for computing the (noise-free) measurement of a radar are the phase gradient method (PGM), originating in [25] and the Poynting vector method (PVM), originating in [26].

The differences and similarities between the PGM and PVM techniques are debated in [27–29]. Here, the PGM method is chosen due to its simpler formulation. The PGM method is based on the notion that the measured range, direction, and range rate of the target are related to derivatives of the phase of the received signal. This is demonstrated for a single point scatterer in a monostatic scenario [30] and Section 2 derives the same thing for a bistatic scenario.

The solutions derived in this report assume far-field targets. Some expressions for glint for near-field targets are given in [31] and much more sophisticated (and complicated) polarimetric electromagnetic solutions for generally shaped targets or surfaces are available, such as [32]. The majority of the literature addresses glint purely as a phenomenon affecting direction measurements. Thus, the notion of "bistatic" glint discussed in this paper might sound a bit odd, because the location of the transmitter does not affect the angular component of glint (not considering how the radar cross section [RCS] of scatterers might vary). However, range glint is a phenomenon that exists and is discussed, for example, in [33–37]. There is, however, less documentation on how well the PGM or PVM methods model range and range rate glint biases with the outputs of modern detection algorithms.

Glint errors for multiple scatterers in the monostatic case are considered in 2D in [34]. This paper derives a more practicable bistatic solution in 2D and 3D for an arbitrary number of scatterers in Section 3 using Cartesian coordinates rather than the polar coordinates used in [34]. In [36], bistatic and monostatic solutions for the range and angle glint of two unresolved scatterers in 2D are considered using the PGM method. However, the bistatic solution is based on an incorrect expression of the range gradient (a monostatic expression was used instead of a bistatic expression). In [4, Ch. 1.2], monostatic solutions in 2D are considered. Section 4 provides similar 2D expressions using the Cartesian solution of this paper. Section 4 also derives glint offset extrema in 2D and plots a number of examples.

The results of this paper are concluded in Section 5.

2. THE SINGLE POINT-SCATTERER CASE

Under a narrowband model (focussing on a single frequency) and considering only a single polarization, the (real) received signal model in the time domain is

$$e_1(t) = E_1 \cos\left(\omega\left(t - t_1\right) + \delta_1\right) \tag{1}$$

where t is time, t_1 is the delay from the transmitter, to the target and then to the receiver, E_1 is the (real, positive) received signal amplitude, and δ_1 is a phase shift. The angular frequency ω is

$$\omega = 2\pi f \tag{2}$$
$$= \frac{2\pi c}{\lambda} \tag{3}$$

where f is the frequency of the narrowband wave, c is the propagation speed (assumed constant over the entire path) and λ is the wavelength. Equation (1) can be rewritten as

$$e_1(t) = E_1 \cos(\omega t - \psi_1) \tag{4}$$
$$\psi_1 = \omega t_1 - \delta_1 \tag{5}$$

Let $\mathbf{l}_{\mathrm{Tx}}$, $\mathbf{l}_{\mathrm{Rx}}$, and $\mathbf{t}_1$ be the 2×1 (in 2D space) or 3×1 (in 3D space) locations of the transmitter, receiver and the single point scatterer of the target. The time delay is thus

$$t_1 = \frac{1}{c}\left(\|\mathbf{t}_1 - \mathbf{l}_{\mathrm{Rx}}\| + \|\mathbf{t}_1 - \mathbf{l}_{\mathrm{Tx}}\|\right) \tag{6}$$

so

$$\psi_1 = \frac{\omega}{c}\left(\|\mathbf{t}_1 - \mathbf{l}_{\mathrm{Rx}}\| + \|\mathbf{t}_1 - \mathbf{l}_{\mathrm{Tx}}\|\right) - \delta_1 \tag{7}$$

We consider the derivatives of the phase ψ_1[1]

$$\frac{\partial \psi_1}{\partial \omega} = \frac{1}{c}\left(\|\mathbf{t}_1 - \mathbf{l}_{\mathrm{Rx}}\| + \|\mathbf{t}_1 - \mathbf{l}_{\mathrm{Tx}}\|\right) \tag{8}$$
$$= \frac{1}{c} r_B \tag{9}$$
$$\frac{\partial^2 \psi_1}{\partial \omega \partial t} = \frac{1}{c}\left(\left(\frac{\mathbf{t}_1 - \mathbf{l}_{\mathrm{Rx}}}{\|\mathbf{t}_1 - \mathbf{l}_{\mathrm{Rx}}\|} + \frac{\mathbf{t}_1 - \mathbf{l}_{\mathrm{Tx}}}{\|\mathbf{t}_1 - \mathbf{l}_{\mathrm{Tx}}\|}\right)' \dot{\mathbf{t}}_1 - \left(\frac{\mathbf{t}_1 - \mathbf{l}_{\mathrm{Rx}}}{\|\mathbf{t}_1 - \mathbf{l}_{\mathrm{Rx}}\|}\right)' \dot{\mathbf{l}}_{\mathrm{Rx}} - \left(\frac{\mathbf{t}_1 - \mathbf{l}_{\mathrm{Tx}}}{\|\mathbf{t}_1 - \mathbf{l}_{\mathrm{Tx}}\|}\right)' \dot{\mathbf{l}}_{\mathrm{Tx}}\right) \tag{10}$$
$$= \frac{1}{c} \dot{r}_B \tag{11}$$
$$\nabla_{\mathbf{l}_{\mathrm{Rx}}} \psi_1 = -\frac{\omega}{c}\left(\frac{\mathbf{t}_1 - \mathbf{l}_{\mathrm{Rx}}}{\|\mathbf{t}_1 - \mathbf{l}_{\mathrm{Rx}}\|}\right) \tag{12}$$
$$= -\frac{\omega}{c}\mathbf{u} \tag{13}$$

where $\dot{\mathbf{l}}_{\mathrm{Tx}}$, $\dot{\mathbf{l}}_{\mathrm{Tx}}$ and $\dot{\mathbf{t}}_1$ are the respective velocity vectors of the transmitter, receiver, and target, and r_B is the bistatic range to the target, $\dot{r}_B$ is the bistatic range rate, and $\mathbf{u}$ is a unit vector from the receiver to the target.

[1] In [30, 34], the partial derivative used for range is taken with respect to f. In [36], it is with respect to ω. We take it with respect to ω to avoid multiplicative constants.

Consequently the gradients relate to typical target parameters

$$r_B = c\frac{\partial \psi_1}{\partial \omega} \tag{14}$$

$$\dot{r}_B = c\frac{\partial^2 \psi_1}{\partial \omega \partial t} \tag{15}$$

$$\mathbf{u} = -\frac{c}{\omega}\nabla_{\mathbf{l}_{\mathrm{Rx}}}\psi_1 \tag{16}$$

where the unit direction vector can be converted into whatever rotated measurement coordinate system is used by the receiver.

The combination of r_B and $\mathbf{u}$ can be converted into a target position in global coordinates [38, 39] is

$$\mathbf{t}_1 = \mathbf{l}_{\mathrm{Rx}} + \frac{r_B^2 - \|\mathbf{l}_{\mathrm{Tx}} - \mathbf{l}_{\mathrm{Rx}}\|^2}{2\left(r_B - \mathbf{u}'\left(\mathbf{l}_{\mathrm{Tx}} - \mathbf{l}_{\mathrm{Rx}}\right)\right)}\mathbf{u} \tag{17}$$

The results in this section have essentially shown some of the same basic things shown in [30], but in a Cartesian, bistatic manner and without being beholden to a 2D coordinate system.

3. THE MULTIPLE POINT-SCATTERER CASE

The notion behind the PGM is that the same gradients that lead to (noise-free) range, range rate, and direction parameters for a single scatterer can adequately describe what one would expect to measure given multiple, unresolved, closely-spaced scatterers when no superresolution is performed. Note that the general idea is that the gradient with respect to $\mathbf{l}_{\mathrm{Rx}}$ will point in the apparent direction of the receiver from the target (as in (13)). However, the scale factors will be different. Thus, to get a unit vector, it must be normalized.

Let there be a total of N unresolved scatterers. The received signal model is

$$e_S(t) = \sum_{i=1}^{N} E_i \cos\left(\omega\left(t - t_i\right) + \delta_i\right) \tag{18}$$

$$= \sum_{i=1}^{N} E_i \cos\left(\omega t - \psi_i\right) \tag{19}$$

$$= E_S \cos\left(\omega t - \psi_S\right) \tag{20}$$

where

$$\psi_i = \omega t_i - \delta_i \tag{21}$$

$$= \frac{\omega}{c} r_i - \delta_i \tag{22}$$

and where E_i is the (positive, real) amplitude of the return from the ith scatterer, t_i is the bistatic delay from the transmitter to the ith scatterer to the receiver, and δ_i is the phase shift associated with the return from the ith scatterer. The bistatic range of the ith scatterer is

$$r_i = \|\mathbf{t}_i - \mathbf{l}_{\mathrm{Rx}}\| + \|\mathbf{t}_i - \mathbf{l}_{\mathrm{Tx}}\| \tag{23}$$

The composite magnitude E_S and the composite phase ψ_S are

$$E_S = \sqrt{\left(\sum_{i=1}^{N} E_i \cos(\psi_i)\right)^2 + \left(\sum_{i=1}^{N} E_i \sin(\psi_i)\right)^2} \tag{24}$$

$$\psi_S = \arctan2\left(\sum_{i=1}^{N} E_i \sin(\psi_i), \sum_{i=1}^{N} E_i \cos(\psi_i)\right) \tag{25}$$

where $\mathbf{t}_i$ is the Cartesian location of the ith scatterer. Noting that the scaled partial derivatives of ψ_k can be expressed in terms of ranges are

$$c\frac{\partial \psi_k}{\partial \omega} = r_i \tag{26}$$

$$c\frac{\partial^2 \psi_k}{\partial \omega \partial t} = \frac{\partial r_i}{\partial t} = \dot{r}_i \tag{27}$$

$$-\frac{c}{\omega}\nabla_{\mathbf{l}_{\mathrm{Rx}}}\psi_i = \nabla_{\mathbf{l}_{\mathrm{Rx}}} r_i \tag{28}$$

using

$$\dot{r}_i = \left(\frac{\mathbf{t}_i - \mathbf{l}_{\mathrm{Rx}}}{\|\mathbf{t}_i - \mathbf{l}_{\mathrm{Rx}}\|} + \frac{\mathbf{t}_i - \mathbf{l}_{\mathrm{Tx}}}{\|\mathbf{t}_i - \mathbf{l}_{\mathrm{Tx}}\|}\right)' \dot{\mathbf{t}}_i - \left(\frac{\mathbf{t}_i - \mathbf{l}_{\mathrm{Rx}}}{\|\mathbf{t}_i - \mathbf{l}_{\mathrm{Rx}}\|}\right)' \dot{\mathbf{l}}_{\mathrm{Rx}} - \left(\frac{\mathbf{t}_i - \mathbf{l}_{\mathrm{Tx}}}{\|\mathbf{t}_i - \mathbf{l}_{\mathrm{Tx}}\|}\right)' \dot{\mathbf{l}}_{\mathrm{Tx}} \tag{29}$$

$$\nabla_{\mathbf{l}_{\mathrm{Rx}}} r_i = \frac{\mathbf{t}_i - \mathbf{l}_{\mathrm{Rx}}}{\|\mathbf{t}_i - \mathbf{l}_{\mathrm{Rx}}\|} \tag{30}$$

then the measurement components are obtained from the composite phase gradients as

$$r_B = c\frac{\partial \psi_S}{\partial \omega} = \frac{1}{C^2 + S^2} \sum_{k=1}^{N} E_k \left(C\cos(\psi_k) + S\sin(\psi_k)\right) r_k \tag{31}$$

$$\dot{r}_B = c\frac{\partial^2 \psi_S}{\partial \omega \partial t} = \frac{1}{C^2 + S^2} \sum_{k=1}^{N} E_k \left(C\cos(\psi_k) + S\sin(\psi_k)\right) \dot{r}_k \tag{32}$$

$$\mathbf{u} = \frac{\tilde{\mathbf{u}}}{\|\tilde{\mathbf{u}}\|} \tag{33}$$

$$\tilde{\mathbf{u}} = -\frac{c}{\omega}\nabla_{\mathbf{l}_{\mathrm{Rx}}}\psi_S = \frac{1}{C^2+S^2}\sum_{k=1}^{N} E_k \left(C\cos(\psi_k) + S\sin(\psi_k)\right)\nabla_{\mathbf{l}_{\mathrm{Rx}}} r_k \tag{34}$$

where

$$C = \sum_{i=1}^{N} E_i \cos(\psi_i) \qquad\qquad S = \sum_{i=1}^{N} E_i \sin(\psi_i) \tag{35}$$

Consequently, given the scattering locations, the transmitter and receiver location, and the phase shifts imparted by the scatterers, assuming a lossless atmosphere with a constant permittivity, one can use (31), (32), and (33) to get the apparent measurement. The amplitude and phase of the measurement are from (24) and (25).

4. SIMPLIFIED SOLUTIONS FOR TWO-POINT BISTATIC GLINT

4.1 Simplified Solution

In the case of two scatterers,

$$r_B = c_1 r_1 + c_2 r_2 \tag{36}$$

$$\dot{r}_B = c_1 \dot{r}_1 + c_2 \dot{r}_2 \tag{37}$$

$$\tilde{\mathbf{u}} = c_1\left(\nabla_{\mathbf{l}_{\mathrm{Rx}}} r_1\right) + c_2\left(\nabla_{\mathbf{l}_{\mathrm{Rx}}} r_2\right) \tag{38}$$

$$E_S = \sqrt{E_1^2 + E_2^2 + 2E_1E_2\cos(\Delta)} \tag{39}$$

where

$$c_1 = \frac{E_1\left(E_1 + E_2\cos(\psi_1-\psi_2)\right)}{E_1^2 + E_2^2 + 2E_1E_2\cos(\psi_1-\psi_2)} \tag{40}$$

$$= \frac{z_0^2 + z_0\cos(\Delta)}{z_0^2 + 1 + 2z_0\cos(\Delta)} \tag{41}$$

$$c_2 = \frac{E_2\left(E_2 + E_1\cos(\psi_1-\psi_2)\right)}{E_1^2 + E_2^2 + 2E_1E_2\cos(\psi_1-\psi_2)} \tag{42}$$

$$= \frac{1 + z_0\cos(\Delta)}{z_0^2 + 1 + 2z_0\cos(\Delta)} \tag{43}$$

$$z_0 = \frac{E_1}{E_2} \tag{44}$$

$$\Delta = \psi_1 - \psi_2 \tag{45}$$

Note that if $E_1 = E_2$, then $c_1 = c_2 = \frac{1}{2}$ and the relatives phases $\psi_1 - \psi_2$ do not matter. Additionally, in (36) – (38) c_1 and c_2 are the only values that depend on the ψ_i values.

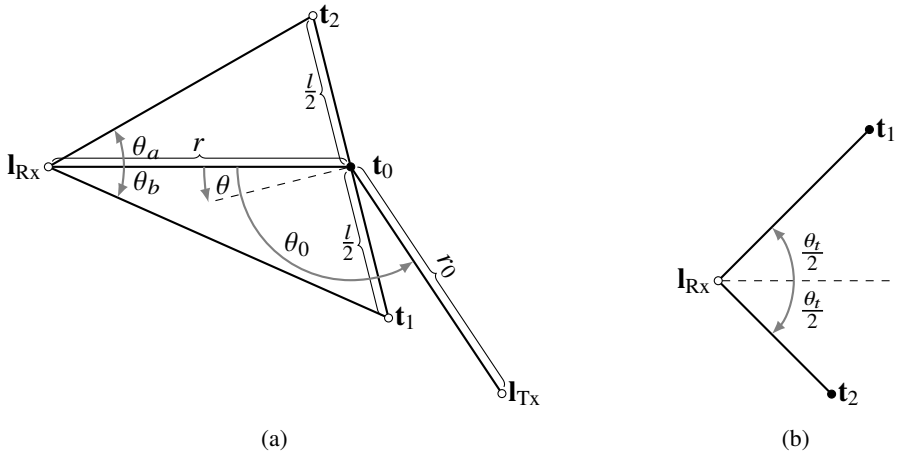

Fig. 1—The two 2D geometries when considering the parameterization for 2D analysis and plotting. General solutions are given in the geometry of (a), whereby the x axis is the midpoint between the scatterers and the scatterers are tiled by an angle θ. However, normally, $\theta_a \neq \theta_b$. Thus, (b) is an alternate geometry ensuring symmetry in those angles, but focussing only on direction in a situation where the transmitter location does not matter.

In order to plot the offsets as a function of a minimal number of parameters in 2D, Fig. 1a, shows the relative geometry between the transmitter, the receiver and the two scatterers for a generic 2D scenario. This is the same geometry formulation used in [36]. The scatterers are a distance l apart. The midpoint between the scatterers $\mathbf{t}_0$ is separated from the receiver by a distance of r and the transmitter by a distance of r_0. The line between $\mathbf{t}_1$ and $\mathbf{t}_2$ is tilted. Using the geometry of Fig. 1, the "correct" solution against which glinted solutions will be compared will consist of the bistatic range and angle values associated with $\mathbf{t}_0$. Additionally, the "correct" range rate will be the range rate associated with a target at $\mathbf{t}_0$ having a velocity that is the average of the velocities of $\mathbf{t}_1$ and $\mathbf{t}_2$.

Letting $\mathbf{l}_{\mathrm{Rx}} = [0, 0]'$ and placing $\mathbf{t}_{\mathrm{mid}} = [r, 0]$ on the x axis, the points $\mathbf{t}_1$, $\mathbf{t}_2$, and $\mathbf{l}_{\mathrm{Tx}}$ can be found as

$$\mathbf{t}_1 = \mathbf{t}_0 - \mathbf{v} \tag{46}$$

$$\mathbf{t}_2 = \mathbf{t}_0 + \mathbf{v} \tag{47}$$

$$\mathbf{v} = \mathbf{M}\begin{bmatrix} 0 \\ \frac{l}{2} \end{bmatrix} \tag{48}$$

$$\mathbf{M}_\theta = \begin{bmatrix} \cos(\theta) & -\sin(\theta) \\ \sin(\theta) & \cos(\theta) \end{bmatrix} \tag{49}$$

$$\mathbf{l}_{\mathrm{Tx}} = \mathbf{t}_0 + \mathbf{M}_{\theta_0}\begin{bmatrix} -r_0 \\ 0 \end{bmatrix} \tag{50}$$

Since the phases δ_1 and δ_2 are typically random, one might want to consider what the maximum errors introduced by the worst-case choice of $\psi_1 - \psi_2$, which is done in the next section.

4.2 Extrema

Let $r_{B,0}$ be the bistatic range of $\mathbf{t}_0$. We want the maximum and minimum offsets in either direction. In terms of range, the cost function to maximize and minimize the offset is

$$\mathcal{L}_r = r_{B,0} - c_1 r_1 - c_2 r_2 \tag{51}$$

The values of Δ such that $d\mathcal{L}_r/d\Delta = 0$ (the stationary points) are

$$\Delta = 0 \tag{52}$$
$$\Delta = \pi \tag{53}$$

Thus, the two extrema that might produce a solution of interest are Δ_1 and Δ_2 which lead to values of

$$\mathcal{L}_{r_B}\big|_{\Delta=0} = r_{B,0} - \frac{r_2 + r_1 z_0}{1 + z_0} \tag{54}$$
$$\mathcal{L}_{r_B}\big|_{\Delta=\pi} = r_{B,0} - \frac{r_2 - r_1 z_0}{1 - z_0} \tag{55}$$

Similarly, due to the equivalent structure of (37), the extrema for range rate are also for $\Delta = 0$ and $\Delta = \pi$ with

$$\mathcal{L}_{\dot{r}_B}\big|_{\Delta=0} = \dot{r}_{B,0} - \frac{\dot{r}_2 + \dot{r}_1 z_0}{1 + z_0} \tag{56}$$
$$\mathcal{L}_{\dot{r}_B}\big|_{\Delta=\pi} = \dot{r}_{B,0} - \frac{\dot{r}_2 - \dot{r}_1 z_0}{1 - z_0} \tag{57}$$

Let the two components of the ith range gradient $\nabla_{\mathbf{l}_{\mathrm{Rx}}} r_i$ be designated $[d_{i,1}, d_{i,2}]'$. Then, th kth component of $\tilde{\mathbf{u}}$ is

$$\tilde{u}_k = c_1 d_{k,1} + c_2 d_{k,2} \tag{58}$$

The implied angle (measured from the x axis, taking the receiver to be at the origin) is thus

$$\phi = \arctan2\left(\tilde{u}_2, \tilde{u}_1\right) \tag{59}$$
$$= \arctan2\left(c_1 d_{1,2} + c_2 d_{2,2}, c_1 d_{1,1} + c_2 d_{2,1}\right) \tag{60}$$

Consider the geometry of Figure 1. In this instance, the angle of $\mathbf{t}_0$ is 0, so any nonzero ϕ is an angular deflection. In this geometry, the angular offset is not going to be over $\pi/2$ radians in magnitude (otherwise the detection would be behind the receiver), so one needn't use a four-quadrant inverse tangent and one can

optimize over $\tan(\phi)$ instead of ϕ directly. Taking $\nabla_{\mathbf{l}_{\mathrm{Rx}}} r_i = [g_{x,i}, g_{y,i}]'$, one can write

$$\tan(\phi) = \frac{g_{y,2} + g_{y,1} z_0^2 + (g_{y,1} + g_{y,2}) z_0 \cos(\Delta)}{g_{x,2} + g_{x,1} z_0^2 + (g_{x,1} + g_{x,2}) z_0 \cos(\Delta)} \tag{61}$$

The zeros of the derivative of $\tan(\phi)$ with respect to Δ, which would correspond to maximum and minimum offsets, are again 0 and π. The corresponding values of $\tan(\phi)$ using (46) and (47) are

$$\tan(\phi)|_{\Delta=0} = \frac{l \cos(\theta)(r_1 - z_0 r_2)}{r_1(2r - l \sin(\theta)) + z_0(2r + l \sin(\theta)) r_2} \tag{62}$$

$$\tan(\phi)|_{\Delta=\pi} = \frac{l \cos(\theta)(r_1 + z_0 r_2)}{r_1(2r - l \sin(\theta)) - z_0(2r + l \sin(\theta)) r_2} \tag{63}$$

with

$$r_1 = \sqrt{l^2 + 4r^2 + 4lr \sin(\theta)} \tag{64}$$

$$r_2 = \sqrt{l^2 + 4r^2 - 4lr \sin(\theta)} \tag{65}$$

Thus, in all instances, the minimum and maximum offsets are obtained with $\Delta = 0$ and $\Delta = \pi$. From (39), the value for $\Delta = 0$ maximizes the received amplitude and for $\Delta = \pi$ minimizes the amplitude. That is

$$E_S|_{\Delta=0} = \sqrt{E_1^2 + E_2^2 + 2E_1 E_2} \tag{66}$$

$$E_S|_{\Delta=\pi} = \sqrt{E_1^2 + E_2^2 - 2E_1 E_2} \tag{67}$$

Note that in the monostatic case, when $z_0 = 1$ (equal strength), if $\theta = 0$, then there is no angular glint error regardless of the phase. Also note that E_S tends to decrease as $|\Delta|$ increases. Thus, in practice, there will exist a maximum value of Δ for which the received amplitude will be large enough for a detection to even be possible. Consequently, a reasonable analysis for a particular sizes target, defined by E_S would only allow Δ to reach a maximum value such that the target could still be detected. If $E_{\min}$ is the minimal detectible amplitude and $E_1 = E_2 = E$, then from (39), the bounds on the magnitude of Δ are

$$|\Delta| \leq \arccos\left(\frac{2E^2 - E_{\min}^2}{2E^2}\right) \tag{68}$$

4.3 Example

Consider a monostatic ($\mathbf{l}_{\mathrm{Rx}} = \mathbf{l}_{\mathrm{Tx}}$) scenario, placing the receiver at the origin and using the geometry of Fig. 1 with $f = 100\,\mathrm{MHz}$, $l = 50\,\mathrm{m}$, $z_0 = 1/2$, and $r = 1\mathrm{km}$, and $E_1 = 1$. Also let the velocities of the scatterers both be set to $\mathbf{t}_1 = [100\,\mathrm{m/s}, 20\,\mathrm{m/s}]'$. Under these conditions, Figure 2 shows the effects of

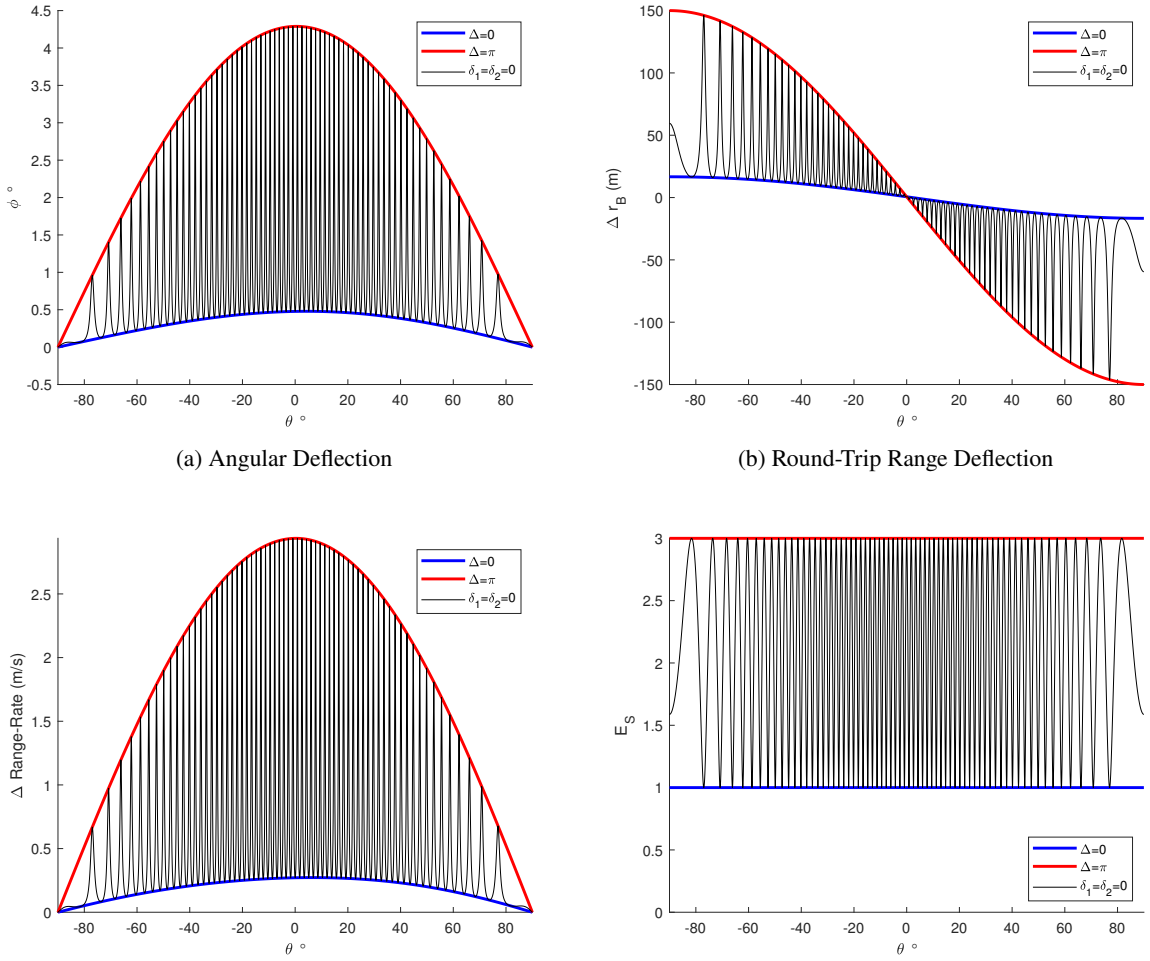

(a) Angular Deflection

(b) Round-Trip Range Deflection

(c) Round-Trip Range-Rate Deflection

(d) Amplitude

Fig. 2—The offset in angle ϕ in (a), the round-trip range offset Δr_B in (b), the round-trip range rate $\Delta \dot{r}_B$ offset, and the amplitude E_S in (b) as a function of the orientation of two scatterers in 2D as well as the upper and lower bounds of Section 4.2. Parameters are given in the text. At $\theta = 0°$, the angular separation between scatterers is about 2.8°, so the angular defection is outside the bounds of the target.

glint in angle, (round-trip) range, range-rate, and amplitude as a function of the relative orientation of the scatterers given by θ.

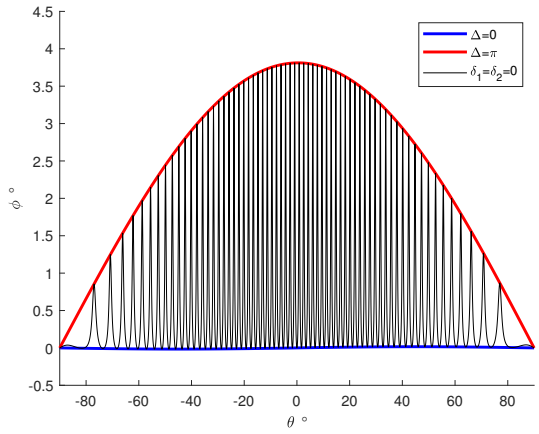

Fig. 3—The sample plot as in Fig. 2a, except the "truth" point has been moved to the weighted average of $\mathbf{t}_1$ and $\mathbf{t}_2$ rather than the unweighted center point.

Note that shifting the "truth" values to a weighted average of $\mathbf{t}_1$ and $\mathbf{t}_2$, does not make the errors average around zero, as can be seen for angle in Fig 3, which is drawn at the same scale as 2a. A nearly identical plot is obtained if one takes as truth a weighted average of the angles of $\mathbf{t}_1$ and $\mathbf{t}_2$ rather than averaging the Cartesian position and then finding the angles. Thus, the assumption in many papers on unresolved target tracking that the unresolved measurement is an unbiased weighted average of the positions of the two unresolved scatterers is incorrect. A bias will exist and the bias depends on z_0.

The plots of angle and range are similar to those given in [36] (though the definition of ϕ is opposite), which uses the same parameters except a frequency of 10 GHz. Increasing the frequency increases the density of the oscillations of the black line, but it does not change the bounds; no bounds were given in [36]. The black line was created using a Δ that varies naturally with ϕ_1 and ϕ_2 for fixed target-induced phase shifts of δ_1 and δ_2. Though such detailed information could be useful in a simulation of the effects of glint induced by two unresolved scatterers, the extremely high sensitivity to the relative orientation θ, indicates that it is not particularly useful for any type of deterministic estimation and the bounds provided here are of more use.

There are practical limits to θ and l. Though l can often large with $\theta = 0$, θ cannot be large enough that the range difference between $\mathbf{t}_1$ and $\mathbf{t}_2$ would mean that the two scatterers would be resolved. Thus, when analyzing only the angular errors, which tend to be the largest errors, it can be useful to consider only the angular offset bounds with respect to the angular separation of the scatterers without explicitly considering $\mathbf{l}$.

Now, consider the same scenario with $z_0 = 1$ as in Fig. 4. Though the amplitude varies, the deflections in angle are minimal and similarly small deflections exist in range and range rate. However, the variations in amplitude E_S can be notable and will reduce the detectability of the target compared to there being only a single scatterer.

5. CONCLUSION

This paper used the phase gradient method to derive expressions for the direction, bistatic range, and bistatic range rate one would expect given an arbitrary number of unresolved scatterers in 2D or 3D. This

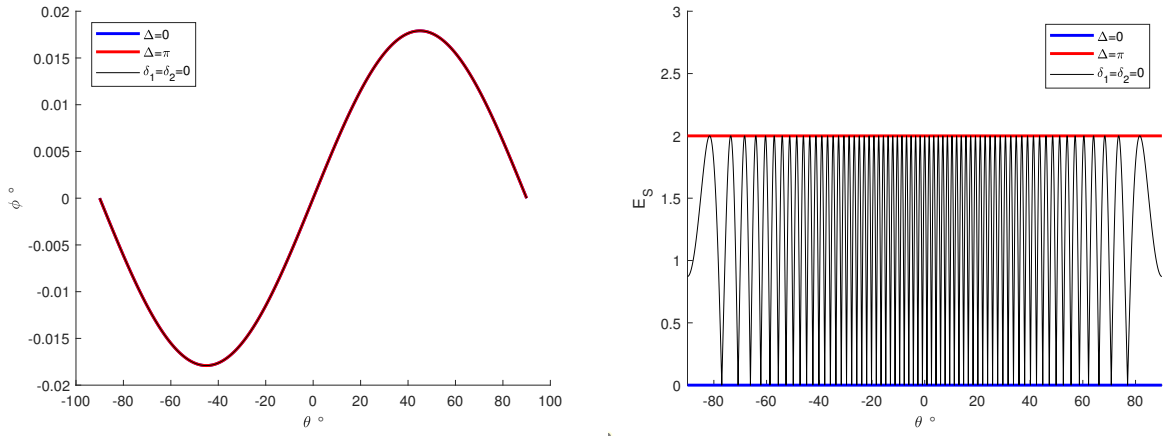

(a) Angular Deflection

(b) Amplitude

Fig. 4—Angular deflection and amplitude under the same scenario as in Fig. 2, but with $z_0 = 1$.

allows one to rapidly simulate glinty-fluctuating returns from a simple target modeled as a collection of point scatterers or from multiple unresolved targets, as might be common when using a radar with a small antenna and poor range resolution, as would be the case with HF and LF systems.

In 2D, a simplified solution is derived, correcting the typos for the bistatic solution in [36]. Additionally, bounds for the maximum and minimum errors in 2D are presented. Since errors can exceed the separation between scatterers, the simple weighting algorithms in unresolved tracking algorithms could be insufficient in some instances and should be reconsidered.

The analysis presented here was generic, simply assuming that no superresolution is performed to detect multiple unresolved scatterers. A more detailed analysis would take into account more assumptions regarding the signal processing algorithms used to obtain the detections.

REFERENCES

1. K. M. Chen, D. P. Nyquist, E. J. Rothwell, L. L. Webb, and B. Drachman, "Radar Target Discrimination by Convolution of Radar Return with Extinction-Pulses and Single-Mode Extraction Signals," *IEEE Transactions on Antennas and Propagation* **34**(7), 896–904 (July 1986).

2. B. Borden, "What is the Radar Tracking "Glint" Problem and Can it Be Solved?," NAWCWPNS TP 8125, Naval Air Warfare Center, Weapons Division, China Lake, CA, May 1993.

3. R. H. Delano, "A Theory of Target Glint or Angular Scintillation in Radar Tracking," *Proceedings of the I.R.E.* **41**(12), 1178–1784 (Dec. 1953).

4. R. V. Ostrovityanov and F. A. Basalov, *Statistical Theory of Extended Radar Targets* (Artech House, Dedham, 1985). Translated from Russian by William F. Barton and David K. Barton.

5. G. A. Hewer and R. D. Martin, "Robust Preprocessing for Kalman Filtering of Glint Noise," *IEEE Transactions on Aerospace and Electronic Systems* **23**(1), 120–128 (Jan. 1987).

6. W. R. Wu, "Target Tracking with Glint Noise," *IEEE Transactions on Aerospace and Electronic Systems* **25**(1), 174–185 (Jan. 1993).

7. E. Daeipour and Y. Bar-Shalom, "An Integrated Multiple Model Approach for Target Tracking with Glint Noise," *IEEE Transactions on Aerospace and Electronic Systems* **31**(2), 706–715 (Apr. 1995).

8. G. Tanner, "Accounting for Glint in Target Tracking," Proceedings of the Proceedings of SPIE: Signal and Data Processing of Small targts, volume 3373, Orlando, FL, 3 Sept. 1998, pp. 144–155.

9. N. Gordon and A. Whitby, "Bayesian Approach to Target Tracking in the Presence of Glint," Proceedings of the Proceedings of SPIE: Signal and Data Processing of Small Targets, volume 2561, San Diego, CA, 1 Sept. 1995, pp. 472–483.

10. I. Bilik and J. Tabrikian, "Maneuvering Target Tracking in the Presence of Glint Using the Nonlinear Gaussian Mixture Kalman Filter," *IEEE Transactions on Aerospace and Electronic Systems* **46**(1), 246–262 (Jan. 2010).

11. D. Svensson, M. Ulmke, and L. Danielsson, "Multitarget Tracking with Partially Unresolved Measurements," Proceedings of the Informatik, Jahrestagung der Gesellschaft für Informatik e.V., volume 2, Leipzig, Germany, 2010, pp. 913–918.

12. D. Svensson, M. Ulmke, and L. Danielsson, "Multitarget Sensor Resolution Model for Arbitrary Target Numbers," Proceedings of the Proceedings of SPIE: Signal and Data Processing of Small Targets, volume 7698, Orlando, FL, 15 Apr. 2010.

13. R. B. Angle, R. L. Streit, and M. Efe, "Multiple Target Tracking wth Unresolved Measurements," *IEEE Signal Processing Letters* **28**, 319–323 (2021).

14. W. Koch, "On Exploiting 'Negative' Sensor Evidence for Target Tracking and Sensor Data Fusion," *Information Fusion* **8**(1), 28–39 (Jan. 2007).

15. W. Koch and G. van Keuk, "Multiple Hypothesis Track Maintenance with Possibly Unresolved Measurements," *IEEE Transactions on Aerospace and Electronic Systems* **33**(3), 883–892 (July 1997).

16. W. Koch, *Tracking and Sensor Data Fusion* (Springer, Heidelberg, 2014).

17. K. Y. Guo, G. L. Xiao, Y. Zhai, and X. Q. Sheng, "Angular Glint Error Simulation Using Attributed Scattering Center Models," *IEEE Access* **6**, 35149–35205 (12 June 2018).

18. X. Zhang, P. K. Willett, and Y. Bar-Shalom, "Monopulse Radar Detection and Localization of Multiple Unresolved Targets via Joint Bin Processing," *IEEE Transactions on Signal Processing* **53**(4), 1225–1236 (Apr. 2005).

19. R. L. Johnson and G. E. Minder, "Comparison of Superresolution Algorthms for Radio Direction Finding," *IEEE transactions on Aerospace and Electronic Systems* **22**(4), 432–442 (July 1986).

20. U. Nickel, *Angular Resolution of Closely-Spaced Targets with Antenna Arrays*, PhD thesis (Rheinisch-Westfälische Technische Hochschule Aachen, Aachen, Germany, 17 Dec. 1982). URL `https://arxiv.org/abs/1908.05308`, Translated from German by Davd F. Crouse and posted to ArXiv.

21. E. Chaumette, U. Nickel, and P. Larzabal, "Detection and Parameter Estimation of Extended Targets Using the Generalized Monopulse Estimator," *IEEE Transactions on Aerospace and Electronic Systems* **48**(4), 3389–3417 (Oct. 2012).

22. U. Nickel, "Overview of Generalized Monopulse Estimation," *IEEE Aerospace and Electronic Systems Magazine* **21**(6), 27–56 (June 2006).

23. U. Nickel, "Radar Target Parameter Esitmation with Antenna Arrays," in S. Haykin, J. Litva, and T. J. Shephers, eds., *Radar Array Processing*, chapter 3 (Springer-Verlag, Berlin, 1993).

24. R. J. McAulay and E. M. Hofstetter, "Barankin Bounds on Parameter Estimation Accuracy Applied to Communications and Radar Problems," ESD-TR-69-49, MIR Lincoln Laboratory, 13 Mar. 1969.

25. D. D. Howard, "Radar Target Angular Scintillation in Tracking and Guidance Systems Based on Echo Signal Phase Front Distortion," Proceedings of the Proceedings of the National Electronics Conference, volume XV, Chicago, IL, 13–15 Oct. 1959.

26. J. H. Dunn and D. D. Howard, "Radar Target Amplitude, Angle, and Doppler Scintillation from Analysis of the Echo Signal Propagating in Space," *IEEE Transactions on Microwave Theory and Techniques* (9), 715–728 (Sept. 1968).

27. P. J. Kajenski, "Comparison of Two Theories of Angle Glint: Polarization Considerations," *IEEE Transactions on Aerospace and Electronic Systems* **42**(1), 206–210 (Jan. 2006).

28. H. C. Yin and P. K. Huang, "Further Comparisons Between Two Concepts of Radar Target Angle Glint," *IEEE Transactions on Aerospace and Electronic Systems* **44**(1), 372–280 (Jan. 2008).

29. W. Chao, Y. Hongchen, and H. Peikang, "Comparison Between Two Concepts of Angular Glint: General Considerations," *Journal of Systems Engineering and Electronics* **19**(4), 635–642 (Aug. 2008).

30. M. I. Skolnik, "Radar Information from the Partial Derivatives of the Echo Signal Phase from a Point Scatterer," 6148, Naval Research Laboratory, 17 Feb. 1988.

31. J. Fan, H. Fan, and H. Xiao, "An Analytic Expression for Near-Field Angular Glint Prediction of Radar Sensor using Far-Field Scattering Center Models," *Progress in Electromagnetics Research M* **30**, 225–238 (2013).

32. W. Wasylkiwskyj and J. Alatishe, "Coherent Scattering from Distributed Targets," Proceedings of the Proceedings of the Microwaves, Radar, and Remote Sensing Symposium, Kiev, Ukraine, 22–28 Sept. 2008.

33. M. P. Jordan, "Range Glint Effects for Homing Interceptor Miss Distance," 642, MIT Lincoln Laboratory, 26 Apr. 1983.

34. V. C. Chen, "Glint Errors Derived from the Partial Derivatives of the Echo Signal Phase for a Distributed Scatterer," NRL/MR/4440–92-6978, Naval Research Laboratory, Washington, DC, 1 May 1992.

35. C. A. Hammer and M. W. Maier, "Methods to Reduce Range Glint in Radars," Proceedings of the Proceedings of the IEEE Aerospace Conference, Snomass, CO, 13 Feb. 1997, pp. 83–102.

36. E. L. Mokole, "Contributions to Radar Tracking Errors for a Two-Point Target Caused by Geometric Approximations," 9349, Naval Research Laboratory, Washington, DC, 19 Sept. 1991.

37. F. Zhao, J. H. Yang, M. Dan, J. Q. Liu, and X. S. Wang, "Detection of Presence of Multiple Unresolved Targets Based on Range Glint," *Acta Electronica Sinica* **36**(12), 2290–2298 (Dec. 2008).

38. D. F. Crouse, "Basic Tracking Using Nonlinear 3D Monostatic and Bistatic Measurements," *IEEE Transactions on Aerospace and Electronic Systems* **29**(4), 4–53 (Aug. 2014).

39. D. F. Crouse, "Particle Flow Solutions Avoiding Stiff Integration," NRL/5340/FR–2021/1, U.S. Naval Research Laboratory, Washington, DC, 25 May 2021.